

Highly luminescent surface-passivated ZnS:Mn nanoparticles by a simple one-step synthesis

Dae-Ryong Jung, Dongyeon Son, Jongmin Kim, Chunjoong Kim, and Byungwoo Park^{a)}

Department of Materials Science and Engineering, and Research Center for Energy Conversion and Storage, Seoul National University, Seoul 151-744, Republic of Korea

(Received 26 August 2008; accepted 2 October 2008; published online 24 October 2008)

Highly luminescent surface-passivated ZnS:Mn nanoparticles were synthesized straightforwardly by a simple liquid-solid-solution method. Compared to the pristine Mn-doped zinc sulfide nanocrystals (quantum efficiency: $\sim 19\%$), the Li-added ZnS:Mn exhibited significantly enhanced luminescence properties (quantum efficiency: $\sim 43\%$). The surface passivation was investigated by x-ray photoelectron spectroscopy, transmission electron microscopy, and by the change in the radiative/nonradiative recombination rates. The photoluminescence enhancement is due to the formation of an effective passivation layer induced by lithium, and consequent suppression of the nonradiative recombination transitions. © 2008 American Institute of Physics. [DOI: 10.1063/1.3007980]

In the past decade, group II-VI semiconductor nanocrystals have been widely studied as luminescent materials.¹⁻⁷ Since a large portion of the atoms are located on or near the surface of the nanoparticles, the surface properties have significant effects on their optical properties. The surface states are likely to trap electrons and/or holes and induce the nonradiative recombination of these charge carriers, leading to the reduction in the luminescence efficiency. Therefore, the surface modification of nanophosphors is an important issue for improving the luminescent efficiency.

Many researchers have studied the surface passivation of a core material by an inorganic shell material. Such shell passivation can lead to the reduction in the surface-related defect states, resulting in more efficient luminescent materials. Several core/shell nanocrystals, such as CdSe/CdS, CdSe/ZnS, and ZnSe/ZnS, have been shown to have much higher quantum efficiencies than the unpassivated ones.⁸⁻¹⁶ Until now, several mechanisms have been proposed for the photoluminescence (PL) enhancement to explain the effect of the passivation layer in the ZnS system. Bol and Meijerink¹⁵ suggested that the photo-oxidation products formed by UV irradiation presumably serve as a good passivating layer on the ZnS:Mn nanoparticles, and reduce the extent of nonradiative recombination. Also, Yang *et al.*¹⁶ examined the formation of ZnSO₄ on the surface of ZnS by UV irradiation. However, the PL enhancement mechanisms of the passivation layer are not yet clear.

Herein, we report highly luminescent surface-passivated ZnS:Mn nanoparticles synthesized by a simple one-step method. The PL enhancement afforded by the formation of the passivation layer induced by lithium addition was studied, considering its effect on the radiative/nonradiative recombination rates.

The ZnS:Mn nanophosphors were synthesized using a liquid-solid-solution method for preparing nearly monodispersed nanoparticles.¹⁷⁻¹⁹ First, Zn(CH₃COO)₂·2H₂O (0.66 g) was dissolved in distilled water (10 ml) and stirred to achieve its complete dissolution. As a sulfur source, 0.225 g of thioacetamide (CH₃CSNH₂) was dissolved in ethanol (10 ml), and Mn(NO₃)₂ (0.05 g) and LiOH·H₂O were

prepared in distilled water. Zinc acetate solution was added to the autoclave, and manganese nitrate solution was poured into the vessel. Then, the lithium-precursor solution was added to the autoclave. Both 0.1 g of sodium linoleate [(C₁₇H₃₁)COONa] and the thioacetamide solution were added to the resultant solution, and 0.2 ml of linoleic acid [(C₁₇H₃₁)COOH] was added to control the reaction rate. The autoclave was sealed and heated at 90 °C for 10 h. The resultants were centrifuged, cleaned several times with ethanol, and dried at 60 °C for 5 h. To remove both the water and organic capping, all of the powders were annealed at 450 °C for 3 h in air.

The nanostructures of the ZnS:Mn nanoparticles were analyzed by high-resolution transmission electron microscopy (TEM) (JEM-3010, JEOL), x-ray diffraction (XRD) (M18XHF-SRA, MAC Science), and inductively coupled plasma (ICP) (ICP-1000IV, Shimadzu). The emission spectra were recorded on a spectrofluorometer (FP-6500, JASCO), and the chemical-bond states were analyzed by x-ray photoemission spectroscopy (XPS) (AXIS, Kratos) with Mg K α radiation. The time-resolved PL decay curves were measured by a picosecond laser system (FLS-920, Edinburgh).

The XRD patterns of the ZnS:Mn nanoparticles with different Li-precursor concentrations (0, 1, 2, 5, 10, 15, and 20 at. %) were measured, as shown in Fig. S1 (see Ref. 20). The concentration of lithium was confirmed by ICP, exhibiting 0, 0.04, 0.08, 0.18, 0.34, 0.34, and 0.35 at. %, respectively. All of the samples exhibited a cubic zinc-blende structure, and there were no secondary phases in the ZnS:Mn nanocrystals. Table S1 (see Ref. 20) shows the nanoparticle size and nonuniform distribution of local strain (crystallinity) estimated from the Scherrer equation of Δk versus k [the scattering vector $k=(4\pi/\lambda)\sin\theta$]. The three peaks were fitted using a double-peak Lorentzian function for $K\alpha_1$ and $K\alpha_2$, and the average sizes of the Li-added ZnS:Mn nanoparticles (at $k=0$) were 7.5 ± 0.5 nm. The nonuniform distribution of local strain ($\Delta d/d$ with $k=2\pi/d$) was obtained from the slope of the Δk versus k plot,^{17,21,22} as shown in Fig. S2 (see Ref. 20).

The PL emission spectra of the Li-added ZnS:Mn nanoparticles were measured with 325 nm excitation at room temperature, as shown in Fig. 1. To investigate the Li-addition

^{a)}Electronic mail: byungwoo@snu.ac.kr.

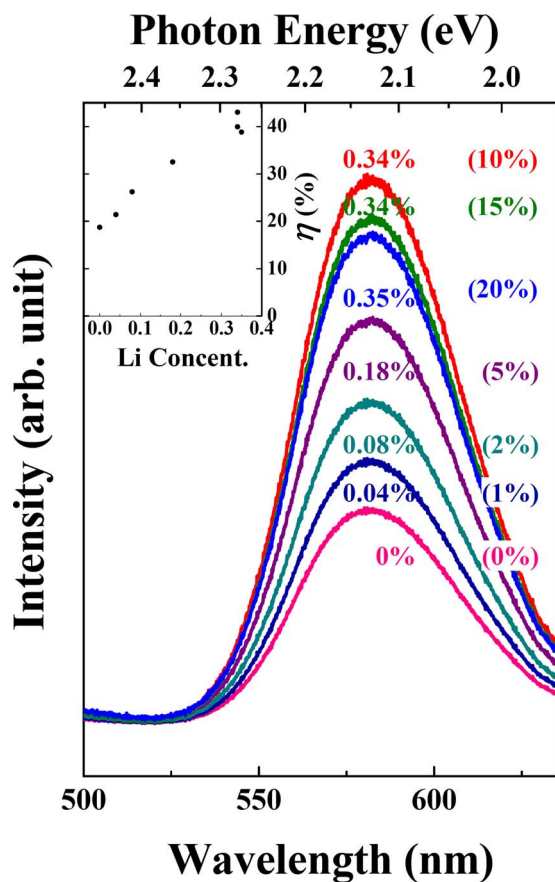


FIG. 1. (Color online) PL spectra of the 450 °C-annealed ZnS:Mn nanoparticles with different Li additions. (The value in the parenthesis is the Li-precursor concentration, and the Mn concentration for all of the samples is 1.0 at. %).

effect, the Mn concentration was controlled at 1.0 at. %. (The emission peak at ~ 580 nm is attributed to the ${}^4T_1 - {}^6A_1$ transition of the Mn^{2+} ion.) The PL intensities were improved with increasing the Li concentration, and the ZnS:Mn nanoparticles with 0.34 at. % (10 at. % precursor concentration) represented a strong Mn-emission peak. However, a decrease in the luminescence intensity was observed at high Li concentrations, probably due to the existence of an optimum thickness for the passivation layer.

To study the luminescence properties quantitatively, the quantum efficiency of the ZnS:Mn sample was estimated using a commercial $Y_2O_3:Eu^{3+}$ phosphor (quantum efficiency of approximately 90% for an excitation wavelength of 250 nm), by assuming negligible absorbance differences.⁸ Accordingly, the quantum efficiency (η) of the 0.34 at. % Li-added nanoparticles ($\sim 43\%$) was much higher than that of bare ZnS:Mn ($\sim 19\%$).

To study the PL enhancement of the Li-added ZnS:Mn nanophosphors, the nanoparticle size, local strain, doping concentration, and capping effect were examined. The ZnS:Mn nanoparticles with different Li concentrations (0, 1, 2, 5, 10, 15, and 20% Li precursors) showed size deviations within $\pm 5\%$ (Table S1, see Ref. 20), and the size effect was relatively small. The nonuniform distribution of local strain used to compare the crystallinity of the ZnS:Mn nanophosphors, as shown in Table S1 (see Ref. 20), exhibited a similar value for all the Li-added nanoparticles. The degree of Mn-activator doping was confirmed by ICP, being

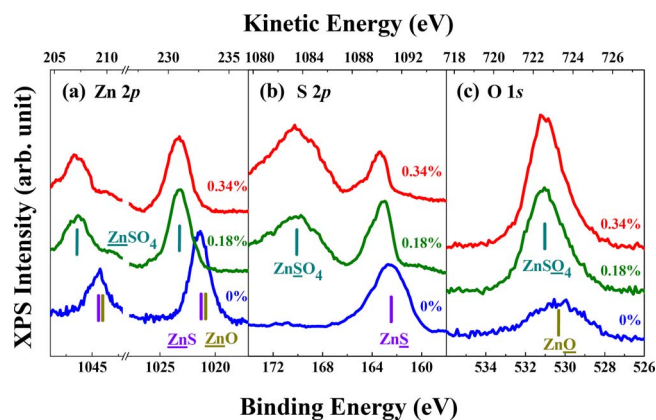


FIG. 2. (Color online) X-ray photoemission spectra corresponding to (a) Zn 2p, (b) S 2p, and (c) O 1s for the ZnS:Mn nanocrystals with different Li concentrations.

1.01 ± 0.03 at. % for all of the samples. Consequently, the variations in the effect of the three factors (the nanoparticle size, the crystallinity, and the Mn concentration) on the PL properties were minimized in this study, thereby allowing us to focus on the effect of passivation layer on the luminescence properties.

Figure 2 shows the XPS spectra for the Zn 2p, S 2p, and O 1s of the ZnS:Mn nanocrystals. To characterize the passivation layer, the XPS analysis was performed at different Li concentrations (0, 0.18, and 0.34 at. %). The marked peak positions were from the standard samples of ZnS, ZnSO₄, and ZnO. The binding energies of the Zn 2p peaks in Li-free ZnS:Mn were close to the values of the pure ZnS or ZnO. However, the Zn 2p peaks of the Li-added ZnS:Mn nanoparticles were shifted by ~ 2 eV in the case of Li addition. The binding energies of the Zn 2p_{1/2} and Zn 2p_{3/2} peaks (~ 1046 and ~ 1023 eV) in the Li-added ZnS:Mn nanoparticles were quite close to the peak positions of the standard ZnSO₄.¹⁶

In Fig. 2(b), the S 2p peak of the Li-free sample only showed a peak at ~ 163 eV. However, the Li-added ZnS:Mn nanocrystals showed two peaks, of which the peak at ~ 170 eV corresponds to the sulfur peak of ZnSO₄. Moreover, the Li-added ZnS:Mn nanocrystals showed a strong O 1s peak at ~ 531 eV, corresponding to the oxygen peak of ZnSO₄, as shown in Fig. 2(c). On the other hand, the O 1s peak of the pristine ZnS nanoparticles had a weak intensity resulting from the Zn–O bonding. (ZnO can be slightly formed at the surface, due to annealing.) Consequently, the XPS results indicated the formation of a passivation layer (ZnSO₄) in the Li-added nanoparticles. It is known that alkali metals are used as additives or catalysts to form the oxide species due to their large reduction activities.^{23–25} In our case, lithium near the nanoparticle surface is expected to play important roles for forming oxide species by the reaction with oxygen in air, while the exact kinetic paths need to be clarified. A related inorganic-passivation layer was also reportedly formed by UV irradiation on nanoparticles in air or in various solvents.^{3,11,15,16}

In the Li-added ZnS:Mn nanoparticles, the Zn 2p peaks attributed to ZnS disappeared (with a binding energy of ~ 1021 eV), while the S 2p peak remained (with a binding energy of ~ 163 eV). From these, the thickness of passivation layer (ZnSO₄) was roughly estimated to be ~ 1 nm, considering the kinetic energy (with Mg K α radiation of

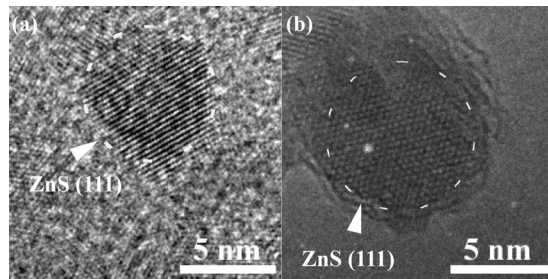


FIG. 3. TEM images of ZnS:Mn nanoparticles (a) without Li (~ 7.2 nm) and (b) with 0.34 at. % Li (~ 7.6 nm).

1253.6 eV) and the electron escape depth. High-resolution TEM (Fig. 3) showed the presence of an approximately 1 nm thick amorphous coating layer in the case of the Li-added ZnS:Mn, in contrast to the Li-free nanoparticles.¹⁷

For the carrier dynamics in the nanoparticles, time-resolved PL measurements were performed. Figure 4 shows the PL decay curves of the ZnS:Mn nanocrystals, and there is a clear difference in the PL decay spectra between the Li-free (0 at. %) and Li-added (0.34 at. %) nanoparticles. The decay curves were analyzed in terms of the radiative/nonradiative recombination rates, as $k_{\text{tot}} = k_{\text{rad}} + k_{\text{nonrad}}$, where k_{tot} , k_{rad} , and k_{nonrad} are the total, radiative, and nonradiative recombination rates, respectively. Also, the quantum efficiency (η) is the ratio of the radiative recombination to the total recombination as

$$\eta = \frac{k_{\text{rad}}}{k_{\text{rad}} + k_{\text{nonrad}}} = k_{\text{rad}}\tau, \quad (1)$$

where the decay time [$\tau = (k_{\text{tot}})^{-1}$] was acquired from a single-exponential fitting of the PL decay curve.

Table I shows the quantum efficiency and radiative/nonradiative recombination rates of both the Li-free (0 at. %) and Li-added (0.34 at. %) nanoparticles. The nonradiative recombination rate was reduced from $3.6 \times 10^8 \text{ s}^{-1}$ (0 at. %) to $1.7 \times 10^8 \text{ s}^{-1}$ (0.34 at. %), indicating that the capping layer greatly enhanced the luminescence efficiency through the restriction of nonradiative loss. The radiative recombination rate was increased from

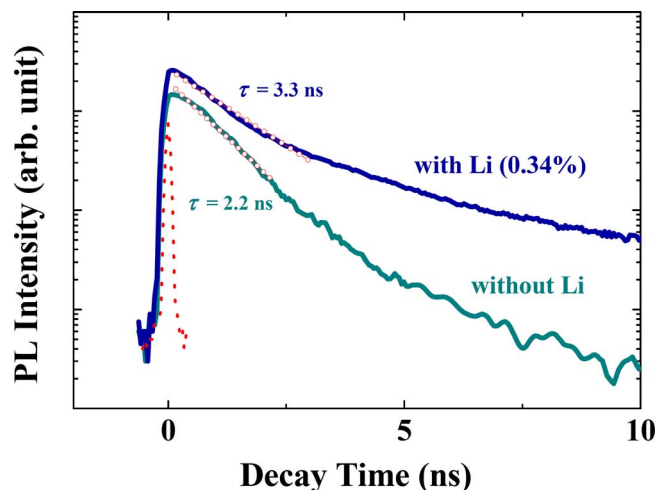


FIG. 4. (Color online) Decay curves of the ZnS:Mn nanocrystals. The samples were excited at 325 nm and recorded at an emission wavelength of 580 nm. The laser pulse is shown as a dotted line.

TABLE I. The contribution of the radiative/nonradiative recombination rates. The decay time (τ) was obtained using a single-exponential fitting [from Eq. (1)].

	Without Li	With 0.34 at. % Li (10 at. % Li precursor)
Quantum efficiency	$\sim 19\%$	$\sim 43\%$
k_{tot}	$4.5 \times 10^8 \text{ s}^{-1}$	$3.0 \times 10^8 \text{ s}^{-1}$
k_{rad}	$0.9 \times 10^8 \text{ s}^{-1}$	$1.3 \times 10^8 \text{ s}^{-1}$
k_{nonrad}	$3.6 \times 10^8 \text{ s}^{-1}$	$1.7 \times 10^8 \text{ s}^{-1}$

$0.9 \times 10^8 \text{ s}^{-1}$ (0 at. %) to $1.3 \times 10^8 \text{ s}^{-1}$ (0.34 at. %), probably due to the near-surface Mn^{2+} ions (within ~ 0.5 nm thickness from the nanoparticle surface), activated by the passivation layer.

In conclusion, surface-passivated ZnS:Mn nanoparticles with a diameter of 7.5 ± 0.5 nm were synthesized by a simple one-step method. The Li-added ZnS:Mn nanocrystals ($\eta \cong 43\%$) exhibited significantly improved luminescence properties compared to the pure Mn-doped zinc sulfide ($\eta \cong 19\%$). The enhanced PL properties are attributed to the effective suppression of nonradiative recombination by the surface-passivation layer.

This work was supported by the ERC program of MOST/KOSEF (No. R11-2002-102-00000-0).

¹S. C. Erwin, L. Zu, M. I. Haftel, A. L. Efros, T. A. Kennedy, and D. J. Norris, *Nature (London)* **436**, 91 (2005).

²V. L. Colvin, M. C. Schlamp, and A. P. Alivisatos, *Nature (London)* **370**, 354 (1994).

³R. N. Bhargava and D. Gallagher, *Phys. Rev. Lett.* **72**, 416 (1994).

⁴N. S. Norberg and D. R. Gamelin, *J. Phys. Chem. B* **109**, 20810 (2005).

⁵P. V. Radovanovic, N. S. Norberg, K. E. McNally, and D. R. Gamelin, *J. Am. Chem. Soc.* **124**, 15192 (2002).

⁶M. L. Pang, W. Y. Shen, and J. Lin, *J. Appl. Phys.* **97**, 033511 (2005).

⁷J. Y. Cho, Y. R. Do, and Y.-D. Huh, *Appl. Phys. Lett.* **89**, 131915 (2006).

⁸A. A. Bol and A. Meijerink, *J. Phys. Chem. B* **105**, 10197 (2001).

⁹K. T. Shimizu, W. K. Woo, B. R. Fisher, H. J. Eisler, and M. G. Bawendi, *Phys. Rev. Lett.* **89**, 117401 (2002).

¹⁰M. Mattila, T. Hakkarainen, H. Lipsanen, H. Jiang, and E. I. Kauppinen, *Appl. Phys. Lett.* **90**, 033101 (2007).

¹¹N. Myung, Y. Bae, and A. J. Bard, *Nano Lett.* **3**, 747 (2003).

¹²J. Zhuang, X. Zhang, G. Wang, D. Li, W. Yang, and T. Li, *J. Mater. Chem.* **13**, 1853 (2003).

¹³E. Jang, S. Jun, Y. Chung, and L. Pu, *J. Phys. Chem. B* **108**, 4597 (2004).

¹⁴H. Yang and P. H. Holloway, *Adv. Funct. Mater.* **14**, 152 (2004).

¹⁵A. A. Bol and A. Meijerink, *J. Phys. Chem. B* **105**, 10203 (2001).

¹⁶H. Yang, P. H. Holloway, G. Cunningham, and K. S. Schanze, *J. Chem. Phys.* **121**, 10233 (2004).

¹⁷D. Son, D.-R. Jung, J. Kim, T. Moon, C. Kim, and B. Park, *Appl. Phys. Lett.* **90**, 101910 (2007).

¹⁸X. Wang, J. Zhuang, Q. Peng, and Y. Li, *Nature (London)* **437**, 121 (2005).

¹⁹J. Cho, Y.-W. Kim, B. Kim, J.-G. Lee, and B. Park, *Angew. Chem., Int. Ed.* **42**, 1618 (2003); C. Kim, M. Noh, M. Choi, J. Cho, and B. Park, *Chem. Mater.* **17**, 3297 (2005).

²⁰See EPAPS Document No. E-APPLAB-93-066843 for supplemental materials (S1, S2, Table S1). For more information on EPAPS, see <http://www.aip.org/pubservs/epaps.html>.

²¹T. Moon, S.-T. Hwang, D.-R. Jung, D. Son, C. Kim, J. Kim, M. Kang, and B. Park, *J. Phys. Chem. C* **111**, 4164 (2007).

²²T. Kim, J. Oh, B. Park, and K. S. Hong, *Appl. Phys. Lett.* **76**, 3043 (2000).

²³J. H. Song and M. J. Sailor, *Inorg. Chem.* **38**, 1498 (1999).

²⁴G. Lee, E.-J. Cho, Y. Park, S. Cho, and H.-G. Lee, *Surf. Sci.* **501**, L177 (2002).

²⁵W. C. Fan and A. Ignatiev, *Phys. Rev. B* **41**, 3592 (1990).